

# Coffee-Ring Structure from Dried Graphene Derivative Solutions: A Facile One-Step Fabrication Route for All Graphene-Based Transistors

D. S. Eom, J. Chang, Y. -W. Song, and J. A. Lim\*

Interface Control Research Center, Future Convergence Research Division, Korea Institute of Science and Technology (KIST), Seoul 136-791, Korea

J. T. Han

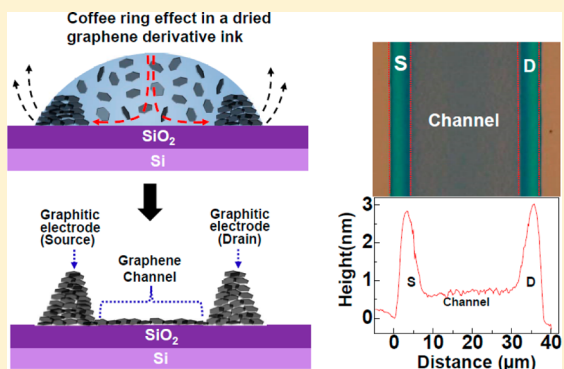
Nano Carbon Materials Research Group, Korea Electrotechnology Research Institute, Changwon 642-120, Korea

H. Kim and K. Cho

Department of Chemical Engineering, Pohang University of Science and Technology (POSTECH), Pohang 790-784, Korea

## Supporting Information

**ABSTRACT:** We demonstrated a coffee-ring structure of graphene derivatives as a one-step solution fabrication route for graphene-based transistors. The key finding is that the coffee-ring structure formed after solvent evaporation of chemically modified graphene nanosheet solutions has an equivalent structure to all graphene-based transistors, the source/drain electrodes and semiconducting channel of which consisted monolithically of graphene nanosheets. These transistors have a thick stack of reduced graphene oxide at the edge of the coffee-ring structure, providing highly conductive thick graphite-like contact as the source and drain electrodes, and the thin film in the midsection of the coffee-ring pattern can simultaneously behave as the semiconducting channel. Here, we provide a holistic approach for achieving coffee-ring graphene-based transistors addressing the entire process flow starting with the coffee-ring structure formation from aqueous graphene oxide dispersion, proceeding through a rapid photoreduction using intensely pulsed white light, and finally a simple cutting of the edge line connections. The degree of graphene oxide reduction was precisely controlled by varying the irradiation energy of pulsed light, which allowed us to systematically investigate its effect on the transistor performances. We confirmed the feasibility of a coffee-ring graphene-based transistor using inkjet printing technique and using chemically reduced graphene oxide dispersions.



## INTRODUCTION

Solvent evaporation driven self-assembly has been recognized as an efficient bottom-up method for producing ordered structures of various nanomaterials including nanoparticles,<sup>1</sup> carbon nanotubes,<sup>2–4</sup> conjugated molecules,<sup>5,6</sup> and zeolites.<sup>7</sup> Recently, growing interest in solution-based printing techniques, such as inkjet printing, and direct-writing patterning methods shed light on the fundamental scientific principles of solvent evaporation behavior for self-assembly of dispersed materials. In fact, droplet evaporation is a complex phenomenon governed by numerous factors including surface wetting properties, solvent compositions, surface tension (Marangoni effect), convective flows, and environmental conditions (i.e., temperature, humidity, and ambient pressure). In general, when a solution droplet dries on a solid surface with fast solvent evaporation, the most frequently observed pattern after drying

is a ring-like deposit marking the perimeter of the initial droplet. This is an outcome of the well-known “coffee-stain” effect described by Deegan and co-workers where the contact line (liquid–substrate–air interface) pinning during drying induces an edge-ward capillary flow to replenish the evaporation loss, and this flow transports the solute materials to its periphery.<sup>8,9</sup> Although the formation of coffee-ring pattern has been acknowledged as an obstacle to be overcome from the viewpoint of producing homogeneous deposits, its unique structure is fascinating for periodic and/or densely packed microstructures.<sup>10</sup> Zhang et al. demonstrated the formation of conductive ring pattern with 5–10 μm widths

Received: July 25, 2014

Revised: September 25, 2014

Published: October 21, 2014



ACS Publications

© 2014 American Chemical Society

27081

dx.doi.org/10.1021/jp507451b | J. Phys. Chem. C 2014, 118, 27081–27090

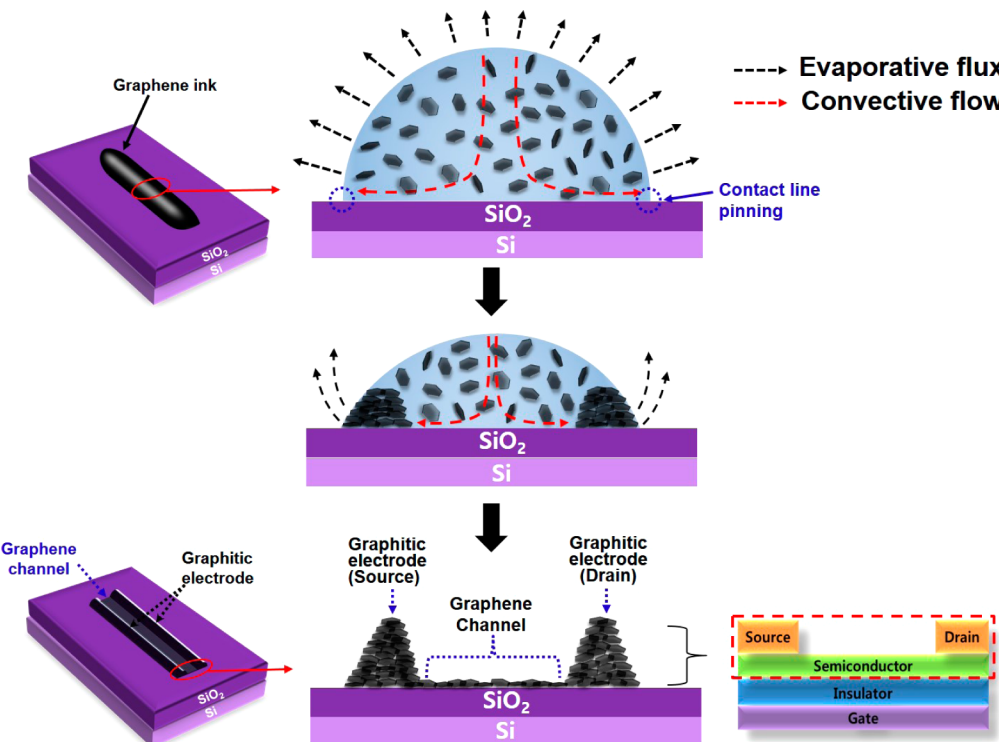


**Figure 1.** (a) Schematic for the coffee-ring pattern formation from graphene oxide dispersions in the solvent evaporation process, which is similar to a transistor configuration with source/drain electrodes and active channel.

utilizing inkjet printing of silver nanoparticles with the coffee-ring effect.<sup>11</sup> More recently, Shimoni et al. demonstrated transparent and conductive films using coffee-ring structure of single wall carbon nanotubes.<sup>12</sup> An inkjet etching technique taking advantage of the coffee-ring effect has been demonstrated for the formation of micropatterns.<sup>13,14</sup>

Recently, graphene has garnered particular interest as a promising carbon-based material with outstanding thermal, mechanical, and electrical properties; thus, research efforts have been devoted toward developing a method for assembling graphene-based nanomaterials into a controllable architecture. While single- up to few-layered graphenes (i.e., ultrathin graphite sheets) with high electrical conductivity and minimized structural defects have been produced by mechanical exfoliation and chemical vapor deposition; reduced graphene oxide (rGO), which is prepared by deoxygenation (i.e., reduction) of chemically exfoliated graphene oxide (GO), is considered as a promising candidate for graphene applications due to its potential for solution processing.<sup>15</sup> Dispersions of rGO and aqueous dispersion of GO allow simple fabrication of homogeneous graphene-based thin films and/or micropatterns using various solution processes including spray coating,<sup>16</sup> dip coating,<sup>17</sup> Langmuir–Blodgett,<sup>18</sup> and rod coating.<sup>19</sup> Furthermore, several research groups achieved rGO-based printable inks and demonstrated inkjet-printed graphene devices such as transistors, sensors, and supercapacitors.<sup>20–24</sup> Evaporation driven self-assembly of rGO (or GO) can provide a cost-effective and facile approach to fabricate periodic graphene patterns. Recently, Kim et al. demonstrated a periodic assembly of rGO platelets by controlled solvent evaporation in a confined geometry.<sup>25</sup> Wang et al. also reported on the formation of regular rGO stripes on hydrophilic substrates using a convective deposition technique.<sup>26</sup> On the basis of the coffee-stain effect of graphene dispersions, Shih et al. developed a size-

dependent separation method to isolate large graphene flakes where the smaller flakes mainly composed the edges of the coffee ring while the particularly larger flakes were located inside the ring.<sup>27</sup>

Herein, we propose a unique strategy for fabrication of a graphene-based transistor in a one-step solution process based on coffee-ring structure of graphene derivatives. The motivation of this work is based on graphene's intrinsic attributes where its electrical properties can be modulated by controlling the number of graphene layers (i.e., thickness of the graphene film). Graphene has a unique electronic structure leading to its zero-band-gap semiconducting nature and simultaneous semimetallic properties. In the case of mono- or bilayered graphenes, the electronic band structure can be modified by constraining the graphene to nanoribbons,<sup>28</sup> applying an electric-field across the bilayer,<sup>29</sup> or introducing chemical functionalization<sup>30</sup> to enhance their semiconducting nature. On the other hand, multilayered graphene shows nearly identical characteristics to graphite, having semimetallic properties with no electric-field-dependent current switching.<sup>31</sup> Graphene's nature allows the fabrication of monolithic graphene–graphite integrated transistors where the graphitic portion of the pattern plays the role of the source (S) and drain (D) electrodes and monolayered or a few-layered graphene (e.g., 2–4 layers) acts as a semiconducting channel.<sup>32,33</sup> The key finding in this work is that the coffee-ring structure of rGO has an equivalent structure to that of all graphene-based transistors, the source/drain electrodes and semiconducting channel of which consisted monolithically of graphene nanosheets, as shown in Figure 1. The thick stack of rGO at the edges of the coffee-ring structure can provide a highly conductive metallic contact for the source and drain electrodes. Concurrently, the thin rGO film in the middle section of the coffee-ring pattern can behave as the semiconductor if the film

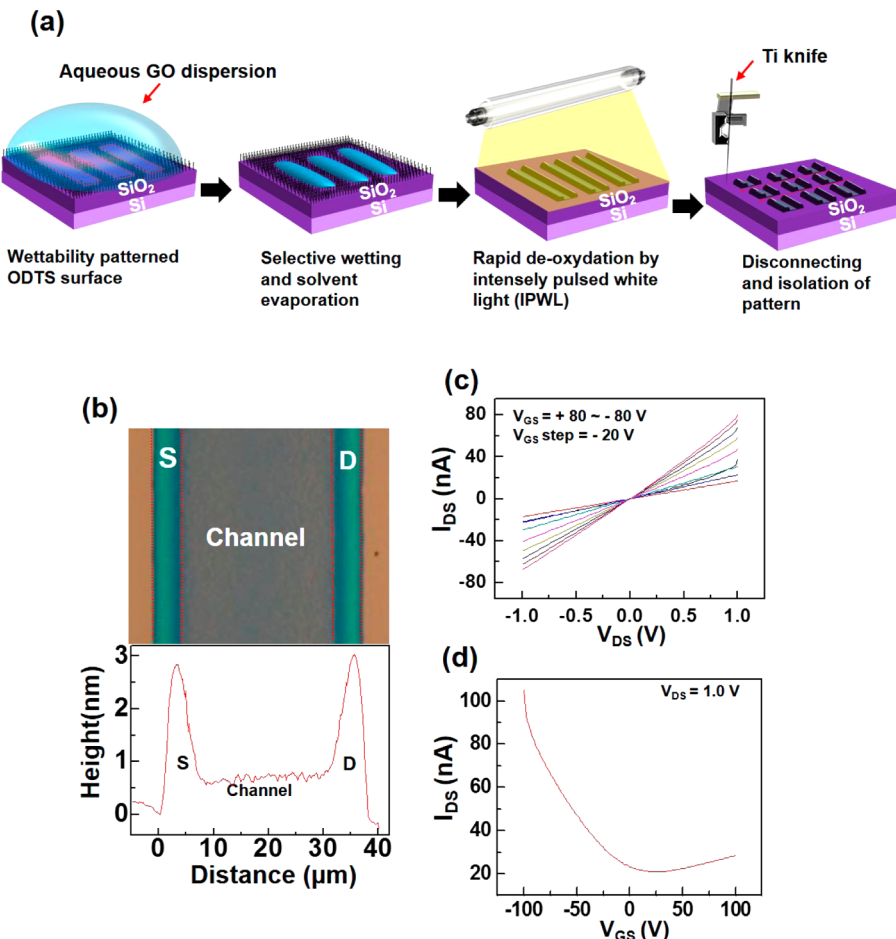


**Figure 2.** (a) Schematic illustrating the fabrication procedure of coffee-ring rGO transistors. (b) OM image (top) and AFM height profile (bottom) of the rGO coffee-ring structure. (c) Output ( $V_{DS}$ - $I_{DS}$ ) and (d) transfer ( $V_{GS}$ - $I_{DS}$ ) curves of a coffee-ring rGO transistor (channel length: 137  $\mu\text{m}$ ; width: 928  $\mu\text{m}$ ; channel thickness: 2.5 nm).

is mainly composed of monolayered or a few-layered rGO nanosheets. This coffee-ring-inspired graphene-based transistor will be called “coffee-ring rGO transistors” from this point on. In this paper, we present a holistic approach for achieving the coffee-ring rGO transistors, addressing the entire process flow. This starts with the formation of the coffee-ring pattern from an aqueous GO dispersion which undergoes rapid photoreduction using intensely pulsed white light (IPWL) followed by a simple cutting of the connecting line edge. The degree of GO reduction was precisely controlled by varying the IPWL irradiation energy, which allowed us to systematically investigate its effect on the transistor performances. A coffee-ring rGO transistor was also achieved using inkjet printing. A coffee-ring pattern using a nonaqueous rGO dispersion was also successfully demonstrated through enhancement of the solvent evaporation rate, which exhibited typical p-type switching behavior.

## ■ EXPERIMENTAL METHODS

**Materials.** To prepare GO nanosheets, first, natural graphite (Alfa Aesar, 99.999% purity, -200 mesh) was oxidized by a modified Hummers method<sup>34</sup> and then exfoliated into GO nanosheets by sonication. Briefly, 10 g of graphite was first added in 230 mL of 70% H<sub>2</sub>SO<sub>4</sub>, followed by slow addition of 30 g of KMnO<sub>4</sub> over 2 h in an ice–water bath under stirring. After the mixture was stirred vigorously for 24 h at room

temperature, 460 mL of deionized water was added, and the solution was stirred for 10 min in an ice–water bath. 25 mL of H<sub>2</sub>O<sub>2</sub> (30 wt % aqueous solution) was then added, and the mixture was precipitated and filtered to obtain the graphite oxide powder, which was then exfoliated into GO nanosheets (500 or 700 mg/L) in water by stirring for 1 h and following bath sonication for 30 min. The redispersed GO suspensions were filtered again through a 5  $\mu\text{m}$  syringe filter to remove large GO flakes which may be nonhomogeneously deposited inside the coffee-ring structure. To obtain rGO solution, water in GO solution was first exchanged into NMP by a rotary evaporator to achieve the stable dispersion of rGO in solution. The chemical reduction of GO (100 mL of 500 mg/L GO solution) was performed by adding hydrazine monohydrate to the GO solution to a final concentration of 4 mM, followed by heating at 100 °C for 5 h.

**Coffee-Ring Structure Formation.** The process selectively switches the substrate surface between hydrophobicity and hydrophilicity by selective UV-ozone exposure. The SiO<sub>2</sub> substrate was cleaned in acetone and ethanol by sonication in a beaker for 15 min. The following piranha cleaning process used a mixture of 70 vol % sulfuric acid (H<sub>2</sub>SO<sub>4</sub>) and 30 vol % hydrogen peroxide (H<sub>2</sub>O<sub>2</sub>) to clean organic residue off the substrates on a hot plate at 120 °C for 30 min. A vacuum-dried reaction flask was charged with anhydrous toluene and the

cleaned substrates. Octadecyltrichlorosilane (ODTS) (10 mM) was then added to the reaction flask and left to self-assemble on the substrate for 1 h under an argon atmosphere. The treated substrate was rinsed with toluene and ethanol several times and then baked in an oven at 120 °C for 20 min. Through a selective exposure to UV-ozone irradiation by a mask placed on top of the ODTS-treated substrate, the exposed portions became hydrophilic while the rest remained hydrophobic. The line pattern widths of the mask were systematically varied from 50 to 200 μm.

**Inkjet Printing Process.** The 0.07 wt % GO solution in DI water was printed on SiO<sub>2</sub> substrates. A home-built inkjet printer was equipped with a single-nozzle drop-on-demand piezoelectric print head (Microfab Jet Drive III), a two-axis motorized positioning system, and a CCD camera aligned with a LED for visualization of the droplet ejection. Single droplets with volumes of 40–50 pL were ejected on demand from the nozzle which has a diameter of 80 μm. The vertical separation between the nozzle and the substrate was typically 0.5 mm.

**Photoreduction of Graphene Oxide by Intensely Pulsed White Light.** A homemade IPWL system was equipped with a xenon flash lamp (PerkinElmer QXF, UK), power supply, capacitors, and a water cooling system. The lamp head was chilled with water to maintain stable operation, and the position of the lamp was adjusted with a z-axis translation stage. The xenon flash lamp emitted a broad spectrum in the range 400–1000 nm. The IPWL system was designed to provide up to 99 pulses on the millisecond scale with a minimum pulse duration of 0.1 ms. The energy of the light was characterized by using a NOVA II laser power meter (OPHIR) and was varied by changing the number of pulses, the pulse duration time (on-time), the free temporal range (off-time), and the voltage. 60 pulses were irradiated on the GO with a 35 ms free-temporal range and 350 V applied voltage, and the pulse duration time was varied from 1.5 to 5 ms to control the total irradiation energy.

**Characterization.** The deposited ring morphologies were characterized with optical microscopy (Olympus, BX2M) and an alpha step surface profiler (KLA Tencor, Alpha Step IQ). Conductive atomic force microscope (Park Systems, XE-100) data were obtained in contact mode under ambient conditions. Silver paste was used to make the contacts to the coffee-ring rGO pattern in c-AFM measurement. The device was grounded, and the voltage of 1.5 V was applied to the tip. XPS data were obtained using a Physical Electronics PHI 5800. The electrical properties of the transistors were characterized by measuring their current–voltage curves (Agilent Technologies, B1500A analyzer) under ambient conditions. The field-effect mobility ( $\mu_{\text{eff}}$ ) was estimated through  $\mu_{\text{eff}} = (\Delta I_{\text{DS}} / \Delta V_{\text{GS}})(L_{\text{ch}}/W_{\text{ch}}C_iV_{\text{DS}})$ , where  $I_{\text{DS}}$  is the drain current,  $V_{\text{GS}}$  is the gate voltage,  $L_{\text{ch}}$  is the channel length,  $W_{\text{ch}}$  is the channel width,  $V_{\text{DS}}$  is the drain voltage, and  $C_i$  is the gate dielectric capacitance. To derive the on–off current ratio, the  $I_{\text{DS}}$  at  $V_{\text{GS}} = -100$  V (or  $-60$  V for coffee-ring rGO transistors prepared by using inkjet printing and nonaqueous rGO dispersion) is divided by the minimum  $I_{\text{DS}}$ .

## RESULTS AND DISCUSSION

The coffee-ring structure of rGO was simply produced using a selective wetting of GO followed by a photoreduction process, as shown in Figure 2a.<sup>35</sup> The silicon dioxide surface was first modified with a hydrophobic self-assembled monolayer, octadecyltrichlorosilane (ODTS), which exhibited a water

contact angle of 102°. The ODTS-treated substrate was exposed to a UV/ozone atmosphere ( $\lambda = 254$  nm, 28 mW/cm<sup>2</sup>, and  $d_{\text{sample-source}} = 5$  cm) for 15 min through a shadow mask to selectively remove the ODTS monolayer in the UV/ozone-exposed areas, creating hydrophilic regions. An aqueous GO dispersion (0.05 wt %) was dropped on the wettability patterned substrate while it was tilted, resulting in the GO dispersion selectively wetted in a lined patterns. The GO nanosheets used in this study was almost monolayer with 1.2 nm thickness and the lateral size ranging from approximately 500 to 1000 μm (see Supporting Information Figure S1a,c). As the drying proceeded in the cylindrical line of GO dispersion at room temperature, the contact lines of the solution pattern maintain their positions due to the pinning force, and outward convective flows are created inside the drop to compensate for the mass loss. These internal flows within the solution move the GO nanosheets to the edges. Eventually, a stack of GO is formed in a coffee-ring structure with a thin midsection surrounded by thick edges. A video of the coffee-ring pattern formation in a drying cylindrical line is provided in Supporting Information Video S1.

Next, the reduction (i.e., deoxygenation) of the GO is required in order to make the coffee ring electrically conductive because GO is inherently insulating. Many studies have suggested that GO can be reduced to rGO by applying chemical reducing agents,<sup>36</sup> a thermal treatment,<sup>37</sup> or by light irradiation, including microwave,<sup>38</sup> laser,<sup>39</sup> or flash light.<sup>40,41</sup> Among these, we focused on photoreduction using flash light which is basically intensely pulsed white light (IPWL). Recently, IPWL has gathered increasing interest as a large-area processable, environmental friendly, and rapid (millisecond) sintering method (or post-treatment process) for various nanomaterials such as metal nanoparticles,<sup>42,43</sup> metal oxide nanoparticles,<sup>44</sup> and polymeric photoactive thin films.<sup>45</sup> IPWL is expected to be a good substitute for a time-intensive and energy-consuming conventional heat treatment. For graphene materials, Cote et al. successfully demonstrated that GO flakes can be instantly reduced by being exposed to photographic camera flash light.<sup>41</sup> In this work, we newly show that one of the most promising aspects of using IPWL for GO reduction is that the degree of reduction can be controlled by altering the pulse energy during irradiation. The effects of the reduction level on the finished device's characteristics will be discussed later. Lastly, to produce a completed transistor, the connections between the source and drain electrodes at both ends of the patterns were severed, and the patterns themselves were then cut to a desired channel width using a handmade Ti cutting tip equipped with an X,Y,Z-axes motor.

Figure 2b shows the optical microscope (OM) image of the coffee-ring rGO transistor (top) and its height profile measured by atomic force microscopy (AFM) (bottom). When using a shadow mask with 50 μm lines and an IPWL irradiation energy of 98 J/cm<sup>2</sup>, a 3 nm high and 8 μm wide stack of rGO formed on the edges of the pattern and the 24 μm wide midsection was a 0.6 nm thick rGO film. This indicates that a monolayer rGO film was successfully obtained within the coffee-ring pattern. The electrical conductance difference between the thick rGO edge stack and the thin flim rGO midsection was tested by measuring their current–voltage ( $I$ – $V$ ) characteristics (see Supporting Information Figure S2). As expected, the current of the edge-stack rGO (1.2 μA) was 10 times higher than that of the thin flim midsection (120 nA) at the same applied voltage (5 V). This result is comparable to a literature report of

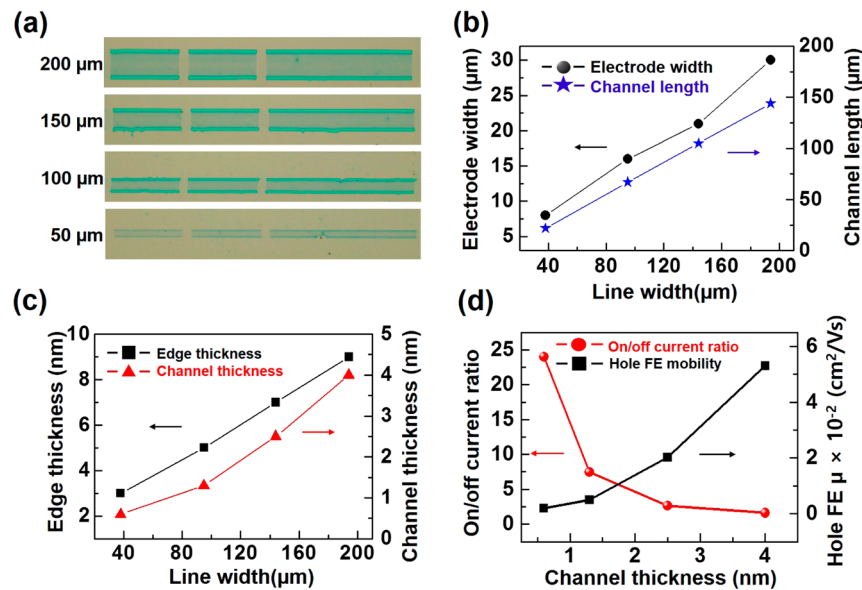


**Figure 3.** (a) OM image of the coffee-ring rGO pattern with various line widths. Effect of line width on the coffee-ring rGO transistor geometry for (b) edge electrode width and channel length and (c) edge thickness and channel thickness. (d) The on/off current ratio and hole mobility of coffee-ring rGO transistors plotted against channel thickness.

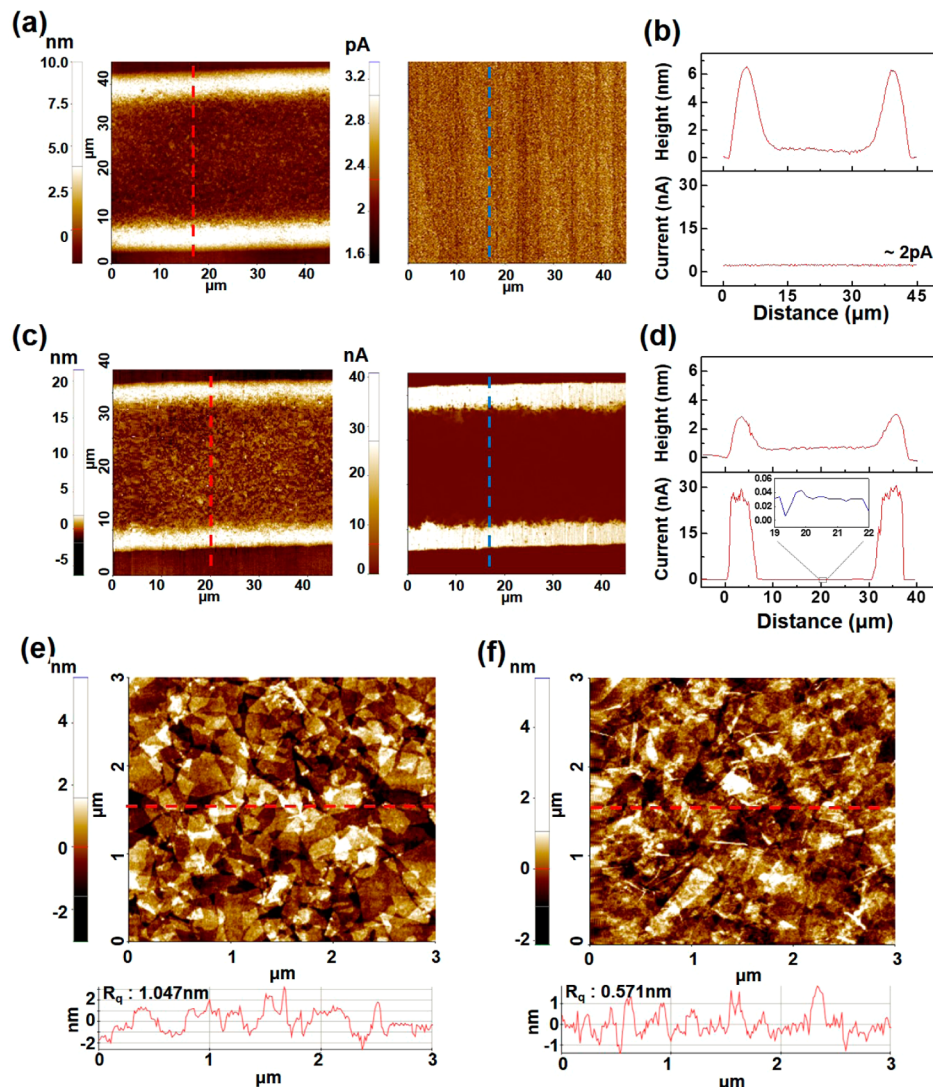
graphene and graphite sheet resistance from a four-point probe measurement, where the resistance reduced by a factor of over 20 as the number of graphene layers increased from  $\sim 2\text{--}4$  to  $\sim 850$ .<sup>33</sup>

Figure 2c,d exhibits the output and transfer characteristics of a coffee-ring rGO transistor responding to the applied gate voltages ( $V_{GS}$ ). A linear behavior at low voltage regime indicates an ohmic contact at the interface between the thin rGO channel and the thick graphite-like electrode. The p-type behavior with a positive charge neutrality point of  $\sim 19$  V and suppressed electron transport seen in this device might be the result of electron trapping by hydroxyl or carboxyl functional groups of the  $\text{SiO}_2$  surface,  $\text{O}_2$  doping, or moisture absorption.<sup>46,47</sup> This electron trapping effect might also give rise to a positive hysteresis (anticlockwise hysteresis) in transfer characteristics on cyclic gate voltage sweep as shown in Supporting Information Figure S3a, which is commonly observed in graphene transistors composed of graphene flakes lying on an insulator and back-gated by silicon substrate.<sup>48</sup> The calculated hole mobility and on–off current ratio were  $1.02 \times 10^{-2} \text{ cm}^2/(\text{V s})$  and 4.3, respectively for a device with a channel length of  $137 \mu\text{m}$ , width of  $928 \mu\text{m}$ , and  $2.5 \text{ nm}$  thickness. As a comparative experiment, when gold was used as the source and drain electrodes for rGO reduced by IPWL, the transistor performance was comparable to that of coffee-ring rGO transistor, showing a hole mobility of  $1.2 \times 10^{-2} \text{ cm}^2/(\text{V s})$  and on/off current ratio of 1.8 (Supporting Information Figure S4). This result suggests that the coffee-ring rGO structure can be used as a one-step fabrication method for graphene-based transistors. Additionally, this indicates that the lower overall mobilities in our devices compared to those achieved for other rGO-based transistors ( $0.01\text{--}200 \text{ cm}^2/(\text{V s})$ ) does not result from the high resistance of the edge stack rGO electrode. Through the morphological and elemental analysis shown in Figures 4 and 5, we found that an incomplete reduction of GO and formation of structural defects after IPWL photoreduction were the main factors lowering the carrier mobility. (Details on the IPWL photoreduction of GO will be addressed later.)

Regarding the reliability of the coffee-ring rGO transistors, the decrease in drain current was observed without change in the on/off current ratio after repeated  $I\text{--}V$  measurements under ambient conditions (see Supporting Information Figure S3b). This indicates that the electrical conductance of rGO film was deteriorated. Although the degradation mechanism is not fully understood, reoxidation of rGO might be responsible for the decrease of conductivity.

Using the proposed method, both the thickness and the width of the graphitic edge and middle rGO thin film can be systematically varied by taking advantage of the fact that the solution amount loaded on the UV-ozone exposed surface increases with increasing line width (i.e., the line width of a shadow mask), as shown in Figure 3a. Figure 3b,c shows the changes in the width and thickness of rGO coffee-ring structure depending on the changes in the pattern line widths. As the line width of a coffee-ring rGO transistor increases from 50 to 200  $\mu\text{m}$ , there was a corresponding increase in the graphitic electrode width (from 8 to 30  $\mu\text{m}$ ), the edge thickness (from 3 to 9 nm), the rGO channel length (from 22 to 144  $\mu\text{m}$ ), and the channel thickness (from 0.6 to 4 nm). As the channel thickness increased from 0.6 to 4 nm, the hole mobility increased from  $1.19 \times 10^{-3}$  to  $5.3 \times 10^{-2} \text{ cm}^2/(\text{V s})$  even though the channel length increased due to the rise in conductivity. However, the on/off ratio dramatically decreased from 24 to 1.6 (Figure 3d). When the channel region consisted of monolayered rGO nanosheets, a high on/off current ratio over 20 was achieved (see Supporting Information Figure S5). The decreased on/off current ratio is caused by the deep overlap between the conduction and the valence bands of the rGO nanosheets resulting from the increased  $\pi\text{--}\pi$  bonds stacking as the channel thickness increases, mimicking the metallic characteristics of graphite.<sup>31,49,50</sup>

In addition, to investigate the threshold GO concentration for formation of coffee-ring rGO transistors, the GO concentration in aqueous solution was varied from 0.01 to 0.1 wt %. The coffee-ring rGO patterns were seemingly observed with an optical microscope as the GO concentration



**Figure 4.** AFM topography (left) and the corresponding current images (right) of coffee-ring pattern (a) GO or (c) rGO. (b) and (d) show the height and current profiles of the GO and rGO coffee-ring patterns, respectively. AFM topography images of the channel region for (e) GO and (f) rGO treated by IPWL irradiation.

decreased to 0.03 wt % (see Supporting Information Figure S6a). At the lower concentration than 0.03 wt %, coffee-ring rGO patterns were not distinguishable under an optical microscope. Figure S6b,c in the Supporting Information shows the electrical performance of coffee-ring rGO transistors with various GO concentrations. Even though the coffee-ring rGO patterns were obtained from a 0.03 wt % GO solution, it did not show electrical switching behavior corresponding to the applied electric field. Except for this exception, the drain current and hole mobilities of the coffee-ring rGO transistors were gradually enhanced with the increasing GO concentrations which is due to the increase of rGO thickness. However, the on/off current ratio adversely decreased as the GO concentration increased, which corresponds with the thickness-dependent performance of coffee-ring rGO transistors as mentioned above.

To confirm the relation between the electrical conductance and thickness of the rGO coffee-ring pattern, conductive atomic force microscopy (c-AFM) was performed. Figure 4 shows a c-AFM image and cross-sectional profiles for a GO coffee-ring pattern fabricated by the selective wetting process with a mask

size of 50 μm, before and after the IPWL photoreduction. Before the reduction of the GO coffee-ring pattern, there was almost no detected electric current (2 pA) regardless of the GO thickness, as shown in Figure 4a,b. In contrast, after the GO photoreduction by exposure to IPWL with an irradiation energy of 98 J/cm<sup>2</sup>, the current profile directly follows the height profile with approximately 30 nA current flowing through the thick (3 nm) edges, while only approximately 40 pA flows through the thin film midsection (0.6 nm) (Figure 4c,d). This indicates that the coffee-ring structure of rGO realizes a thin film transistor configuration with its graphite-like electrodes and rGO semiconductor thin film. Additionally, the observed decrease in the coffee-ring pattern thickness after GO reduction is due to the removal of oxygen-based functional groups. It has been well-known that interspacing distance of GO is 0.71 nm, which decreases to 0.34 nm after reduction.<sup>51</sup> Figures 4e and 4f are the channel region topography images for comparing the morphology before and after the IPWL reduction of GO. Distinct boundaries between individual GO nanosheets are clearly shown in Figure 4e, whereas the rGO prepared by IPWL irradiation shows less defined boundaries

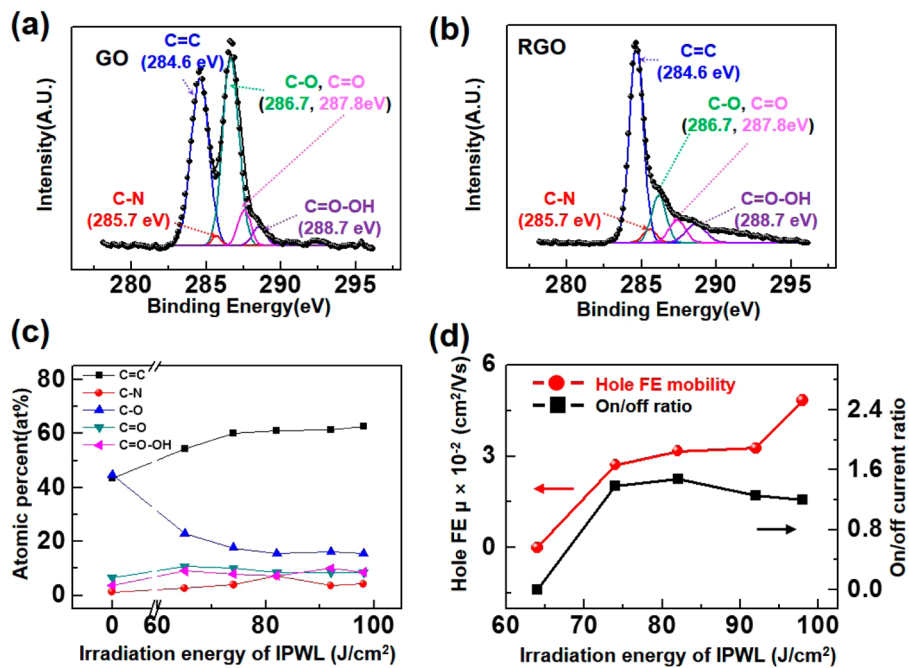


**Figure 5.** C 1s XPS spectra of (a) GO and (b) IPWL-treated rGO. (c) Atomic percent of various functional groups plotted against IPWL irradiation energy. (d) Field-effect mobility and on/off current ratio of coffee-ring rGO transistors plotted against IPWL irradiation energy (channel length: 140  $\mu\text{m}$ ; width: 928  $\mu\text{m}$ ; channel thickness: 2.5 nm).

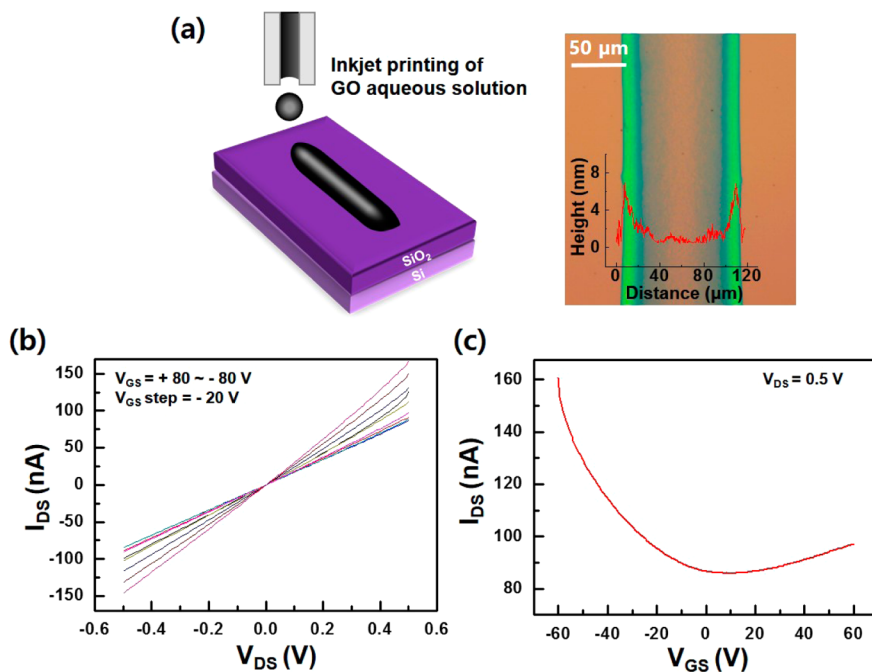


**Figure 6.** (a) Schematic and OM image of inkjet printed coffee-ring rGO transistor (inset: AFM height profile). (b) Output ( $V_{DS}$ – $I_{DS}$ ) and (c) transfer ( $V_{GS}$ – $I_{DS}$ ) curves of the inkjet printed coffee-ring rGO transistor (channel length: 110  $\mu\text{m}$ ; width: 620  $\mu\text{m}$ ; channel thickness: 1.2 nm).

with some folded and torn regions (Figure 4f). The folded and torn areas are due to the rapid thermal expansion during IPWL treatment where the oxygen-containing functional groups are removed, escaping as gas molecules (Supporting Information Figure S1b).<sup>40</sup> This morphology analysis demonstrates that oxygen-based functional groups of GO can be rapidly removed by IPWL irradiation within 1 s, and the resultant structural defects might correspond to the decreased charge carrier mobility in the device performance.

Figure 5 shows the X-ray photoelectron spectroscopy (XPS) analysis measured to investigate the effects of the IPWL irradiation energy on the degree of GO reduction and electrical properties of the coffee-ring rGO transistors. IPWL is consecutive light pulses produced by using a pulse controller and a supercapacitor; the pulse controller triggers the supercapacitor, which delivers electrical current to the lamp within milliseconds. During the IPWL irradiation, high-intensity light energy reaches the sample within a few tens of

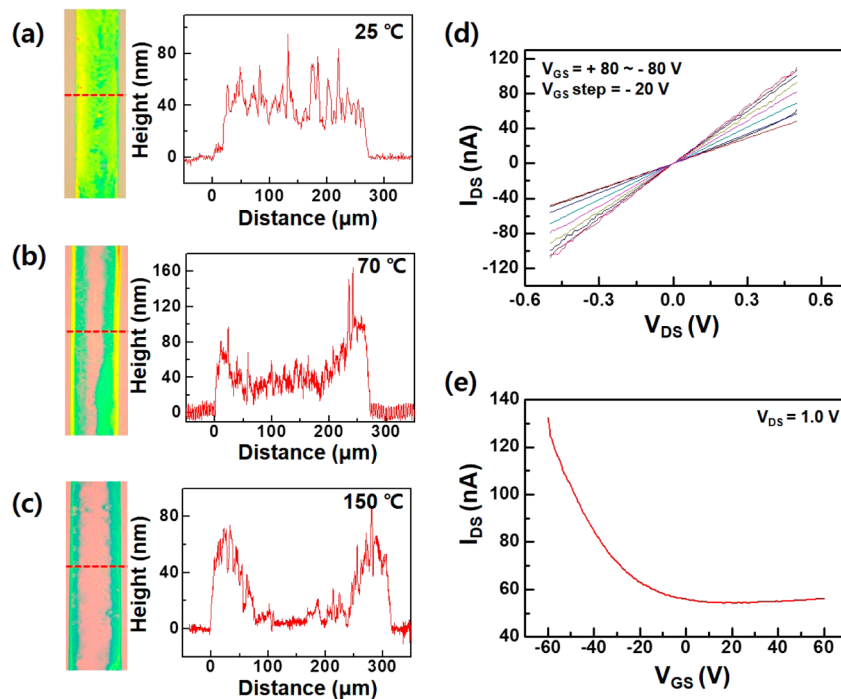


**Figure 7.** OM images (left) and height profiles (right) of rGO line patterns fabricated on substrate at temperatures of (a) 25, (b) 70, and (c) 150 °C. (d) Output ( $V_{DS}$ – $I_{DS}$ ) and (e) transfer ( $V_{GS}$ – $I_{DS}$ ) curves of rGO coffee-ring transistors (channel length: 150  $\mu$ m; width: 926  $\mu$ m; channel thickness: ~3 nm).

milliseconds, which instantly increases the temperature of the sample due to the photothermal effect.<sup>52,53</sup> The irradiation energy can be controlled by varying pulse parameters including the applied voltage, the number of pulses, the pulse duration time, and the free temporal period. In this work, the IPWL irradiation energy was controlled from 65 to 98 J/cm<sup>2</sup> by varying the pulse duration time from 1.5 to 5.0 ms. Notably, the total IPWL exposure time was within 2.0 s. Figure 5a,b shows the C1s XPS spectra of the GO and the rGO prepared by IPWL irradiation with an energy of 98 J/cm<sup>2</sup>. Five types of carbon bonds are observed: C=C, C–N, C–O, C=O, and C=O–OH, corresponding to the peaks at 284.6, 285.7, 286.7, 287.8, and 289.4 eV, respectively.<sup>36</sup> As the IPWL irradiation energy was increased, the C–O bond gradually decreased from 49% to 15%, while the C=C bond increased from 43% to 62% (Figure 5c). This indicates that the IPWL irradiation effectively removes epoxy groups present on the graphene flake's basal plane, and the degree of GO reduction can be controlled by varying the IPWL irradiation energy. The reduction of GO by IPWL irradiation was additionally verified using X-ray diffraction measurement and FT-IR (see Supporting Information Figure S7). In contrast, the C=O and C=O–OH bonds did not appear to have any significant change from the increased irradiation energy. Thus, the low mobility of the IPWL-reduced rGO device may be attributed to residual oxygen-based functional groups on the GO nanosheets after the IPWL process. The effect of GO reduction on the performance of a coffee-ring rGO transistor was tested. With increased irradiation energy, the hole mobility was enhanced from  $2.71 \times 10^{-2}$  to  $4.83 \times 10^{-2}$  cm<sup>2</sup>/(V s), as shown in Figure 5d. The on/off current ratio slightly increased at the irradiation energy between 74 and 82 J/cm<sup>2</sup> and then decreased at the higher energies. It is apparent that the higher IPWL irradiation energy

raises the rGO conductivity by enhancing the recovery of sp<sup>2</sup> hybridization, which in turn reduces the on/off current ratio.

We demonstrated a coffee-ring rGO transistor via a direct-writing pattern using an inkjet printing. The patterns were made with an ink made of GO dispersed in DI water at 0.07 wt %. Figure 6a is the OM image of inkjet printed GO and its height profile obtained by an AFM, confirming that the coffee-ring structure was achieved during the inkjet printing process just as it had for selective wetting. Inkjet printed droplets based on various materials commonly generate coffee-ring deposits because printed droplets with tens of picoliter volumes dry quickly, enhancing the edge-ward convective flows.<sup>54</sup> Recently, it has been reported that there exists a lower limit of droplet size for well-defined coffee-ring formation.<sup>55</sup> Even though the minimum dimension for the coffee-ring rGO formation was not directly suggested in this work, we have confirmed that a coffee-ring structure could be obtained from a single GO droplet with 10 pL volume produced by inkjet printing (Dimatix DMC inkjet cartridge) (see Supporting Information Figure S8). As shown in Figure 6b,c, the operation of the coffee-ring rGO transistor fabricated by inkjet printing was verified by its output and transfer characteristics. When the device has a 110  $\mu$ m channel length, 620  $\mu$ m width, and 1.2 nm channel thickness, the hole mobility and the on/off current ratio were  $3.86 \times 10^{-2}$  cm<sup>2</sup>/(V s) and of 1.7, respectively. This demonstration infers that the proposed coffee-ring rGO transistor can be combined with direct-writing printing techniques, allowing to realization of rGO transistor at specific locations.

We tested the feasibility of a coffee-ring rGO transistor using rGO dispersed ink (0.05 wt %) where rGO is commonly prepared by chemical reduction of GO nanosheets in solutions.<sup>37</sup> As GO nanosheets does not disperse in water after chemical reduction, it had to be dispersed using a polar organic solvent, such as N-methylpyrrolidone (NMP) or

dimethylformamide (DMF),<sup>37</sup> which was achieved by a solvent exchanging method. To induce the coffee-ring effect during the drying process, a fast solvent evaporation with a pinned contact line is preferred. However, the solvents capable of dispersing rGO have high boiling points over 150 °C, weakening the edgeward convective flows induced during solvent drying process. Therefore, it was necessary to utilize an external factor, in this case the drying temperature, to maximize the coffee-ring effect. Patterns produced through the selective wetting process were conducted with a solution of rGO dispersed in NMP. NMP has a boiling point of 202 °C and a low surface tension of 41 mN/m at 25 °C. Figure 7a–c shows the OM images and the height profiles of rGO patterns as increasing the substrate temperature from room temperature to 150 °C. When the rGO solution dried at room temperature, a uniform film of rGO nanosheets formed with no coffee-ring structure. In contrast, as the substrate temperature was raised from 70 to 150 °C, the coffee-ring effect was significantly enhanced. Figures 7d and 7e are the output and the transfer characteristics of the coffee-ring transistor based on rGO prepared at a substrate temperature of 150 °C. The device clearly shows gate bias dependent switching properties with a hole mobility of  $5.2 \times 10^{-2}$  cm<sup>2</sup>/(V s) and an on/off current ratio of 2.4. This indicates that the fabrication of coffee-ring transistors is feasible using non-aqueous rGO dispersions in addition to the GO aqueous dispersions.

## CONCLUSIONS

A novel and simple transistor fabrication method for graphene–graphite integrated transistor has been suggested using the evaporation driven coffee-ring structure of rGO, and the operation of devices built by this method was verified. Coffee-ring rGO transistors were produced using aqueous GO ink by a selective wetting process and an inkjet printing process. Rapid photoreduction of GO using IPWL allows us to convert GO to rGO within 2.0 s and control the degree of GO reduction by varying irradiation energy. Effects of rGO coffee-ring structure and degree of GO reduction on the coffee-ring rGO transistors were systematically studied. Field-effect hole mobility was enhanced as the channel thickness increased from 0.6 to 4 nm and the GO nanosheets recovered its sp<sup>2</sup> hybridization through the photoreduction, while the on/off current ratio was reduced as the channel thickness increased and the degree of GO reduction was high. A coffee-ring rGO transistor using nonaqueous rGO dispersed ink was successfully demonstrated by enhancing the coffee-ring effect at controlled substrate temperature during solvent evaporation. Patterning of graphene-based materials on the arbitrary substrates have been important issues for realization of active devices and heterostructures. This method is advantageous in low cost, possible automation, and short process time.

## ASSOCIATED CONTENT

### Supporting Information

AFM analysis of GO and rGO nanosheets, conductance difference between the thick rGO edge stack and the thin film rGO midsection, gate voltage hysteresis and stability of coffee-ring rGO transistors upon exposure to air, electrical properties of rGO transistors with Au source and drain electrodes, electrical properties of coffee-ring rGO transistors with the channel consisted of monolayered rGO, effect of GO concentration on the coffee-ring formation and device performance, XRD and FT-IR analysis of IPWL-reduced GO,

coffee-ring formation in a single droplet of GO with 10 pL. This material is available free of charge via the Internet at <http://pubs.acs.org>.

## AUTHOR INFORMATION

### Corresponding Author

\*E-mail: [jalim@kist.re.kr](mailto:jalim@kist.re.kr) (J.A.L.).

### Present Address

J.C.: Department of Polymer Science and Engineering, University of Massachusetts, Amherst, MA 01003.

### Notes

The authors declare no competing financial interest.

## ACKNOWLEDGMENTS

This work was supported by Dream Project (2V03380), Institutional Research Program of Korea Institute of Science and Technology (KIST).

## REFERENCES

- (1) Magdassi, S.; Grouchko, M.; Toker, D.; Kamyshny, A.; Balberg, I.; Millo, O. Ring Stain Effect at Room Temperature in Silver Nanoparticles Yields High Electrical Conductivity. *Langmuir* **2005**, *21*, 10264–10267.
- (2) Li, Q.; Zhu, Y. T.; Kinloch, I. A.; Windle, A. H. Self-Organization of Carbon Nanotubes in Evaporating Droplets. *J. Phys. Chem. B* **2006**, *110*, 13926–13930.
- (3) Shastry, T. A.; Seo, J. W.; Lopez, J. J.; Arnold, H. N.; Kelter, J. Z.; Sangwan, V. K.; Lauthon, L. J.; Marks, T. J.; Hersam, M. C. Large-Area, Electronically Monodisperse, Aligned Single-Walled Carbon Nanotube Thin Films Fabricated by Evaporation-Driven Self-Assembly. *Small* **2013**, *9*, 45–51.
- (4) Hong, S. W.; Jeong, W.; Ko, H.; Kessler, M. R.; Tsukruk, V. V.; Lin, Z. Directed Self-Assembly of Gradient Concentric Carbon Nanotube Rings. *Adv. Funct. Mater.* **2008**, *18*, 2114–2122.
- (5) Lim, J. A.; Lee, W. H.; Lee, H. S.; Lee, J. H.; Park, Y. D.; Cho, K. Self-Organization of Ink-Jet-Printed Triisopropylsilylithynyl Pentacene Via Evaporation-Induced Flows in a Drying Droplet. *Adv. Funct. Mater.* **2008**, *18*, 229–234.
- (6) Lim, J. A.; Lee, W. H.; Kwak, D.; Cho, K. Evaporation-Induced Self-Organization of Inkjet-Printed Organic Semiconductors on Surface-Modified Dielectrics for High-Performance Organic Transistors. *Langmuir* **2009**, *25*, 5404–5410.
- (7) Lee, J. A.; Meng, L.; Norris, D. J.; Scriven, L. E.; Tsapatsis, M. Colloidal Crystal Layers of Hexagonal Nanoplates by Convective Assembly. *Langmuir* **2006**, *22*, 5217–5219.
- (8) Deegan, R. D.; Bakajin, O.; Dupont, T. F.; Huber, G.; Nagel, S. R.; Witten, T. A. Capillary Flow as the Cause of Ring Stains from Dried Liquid Drops. *Nature* **1997**, *389*, 827–829.
- (9) Deegan, R. D. Pattern Formation in Drying Drops. *Phys. Rev. E* **2000**, *61*, 475–485.
- (10) Han, W.; Lin, Z. Q. Learning from “Coffee Rings”: Ordered Structures Enabled by Controlled Evaporative Self-Assembly. *Angew. Chem., Int. Ed.* **2012**, *51*, 1534–1546.
- (11) Zhang, Z.; Zhang, X.; Xin, Z.; Deng, M.; Wen, Y.; Song, Y. Controlled Inkjetting of a Conductive Pattern of Silver Nanoparticles Based on the Coffee-Ring Effect. *Adv. Mater.* **2013**, *25*, 6714–6718.
- (12) Shimon, A.; Azoubel, S.; Magdassi, S. Inkjet Printing of Flexible High Performance Carbon Nanotube Transparent Conductive Films by Coffee Ring Effect. *Nanoscale* **2014**, *6*, 11084–11089.
- (13) Kwak, D.; Lim, J. A.; Kang, B.; Lee, W. H.; Cho, K. Self-Organization of Inkjet-Printed Organic Semiconductor Films Prepared in Inkjet-Etched Microwells. *Adv. Funct. Mater.* **2013**, *23*, 5224–5231.
- (14) Zhang, L.; Liu, H.; Zhao, Y.; Sun, X.; Wen, Y.; Guo, Y.; Gao, X.; Di, C. A.; Yu, G.; Liu, Y. Inkjet Printing High-Resolution, Large-Area Graphene Patterns by Coffee-Ring Lithography. *Adv. Mater.* **2012**, *24*, 436–440.

- (15) Eda, G.; Chhowalla, M. Chemically Derived Graphene Oxide: Towards Large-Area Thin-Film Electronics and Optoelectronics. *Adv. Mater.* **2010**, *22*, 2392–2415.
- (16) Blake, P.; Brimicombe, P. D.; Nair, R. R.; Booth, T. J.; Jiang, D.; Schedin, F.; Ponomarenko, L. A.; Morozov, S. V.; Gleeson, H. F.; Hill, E. W.; et al. Graphene-Based Liquid Crystal Device. *Nano Lett.* **2008**, *8*, 1704–1708.
- (17) Wang, X.; Zhi, L. J.; Mullen, K. Transparent, Conductive Graphene Electrodes for Dye-Sensitized Solar Cells. *Nano Lett.* **2008**, *8*, 323–327.
- (18) Li, X. L.; Zhang, G. Y.; Bai, X. D.; Sun, X. M.; Wang, X. R.; Wang, E.; Dai, H. J. Highly Conducting Graphene Sheets and Langmuir-Blodgett Films. *Nat. Nanotechnol.* **2008**, *3*, 538–542.
- (19) Wang, J.; Liang, M. H.; Fang, Y.; Qiu, T. F.; Zhang, J.; Zhi, L. J. Rod-Coating: Towards Large-Area Fabrication of Uniform Reduced Graphene Oxide Films for Flexible Touch Screens. *Adv. Mater.* **2012**, *24*, 2874–2878.
- (20) Torrisi, F.; Hasan, T.; Wu, W. P.; Sun, Z. P.; Lombardo, A.; Kulmala, T. S.; Hsieh, G. W.; Jung, S. J.; Bonaccorso, F.; Paul, P. J.; et al. Inkjet-Printed Graphene Electronics. *ACS Nano* **2012**, *6*, 2992–3006.
- (21) Kong, D.; Le, L. T.; Li, Y.; Zunino, J. L.; Lee, W. Temperature-Dependent Electrical Properties of Graphene Inkjet-Printed on Flexible Materials. *Langmuir* **2012**, *28*, 13467–72.
- (22) Secor, E. B.; Prabhumirashi, P. L.; Puntambekar, K.; Geier, M. L.; Hersam, M. C. Inkjet Printing of High Conductivity, Flexible Graphene Patterns. *J. Phys. Chem. Lett.* **2013**, *4*, 1347–1351.
- (23) Li, J. T.; Ye, F.; Vaziri, S.; Muhammed, M.; Lemme, M. C.; Ostling, M. Efficient Inkjet Printing of Graphene. *Adv. Mater.* **2013**, *25*, 3985–3992.
- (24) Huang, L.; Huang, Y.; Liang, J. J.; Wan, X. J.; Chen, Y. S. Graphene-Based Conducting Inks for Direct Inkjet Printing of Flexible Conductive Patterns and Their Applications in Electric Circuits and Chemical Sensors. *Nano Res.* **2011**, *4*, 675–684.
- (25) Kim, T. Y.; Kwon, S. W.; Park, S. J.; Yoon, D. H.; Suh, K. S.; Yang, W. S. Self-Organized Graphene Patterns. *Adv. Mater.* **2011**, *23*, 2734–2738.
- (26) Wang, Y.; Mino, Y.; Watanabe, S.; Li, D.; Zhang, X. Formation of Regular Stripes of Chemically Converted Graphene on Hydrophilic Substrates. *ACS Appl. Mater. Interfaces* **2013**, *5*, 6176–6181.
- (27) Shih, C. J.; Vijayaraghavan, A.; Krishnan, R.; Sharma, R.; Han, J. H.; Ham, M. H.; Jin, Z.; Lin, S.; Paulus, G. L.; Reuel, N. F.; et al. Bi- and Trilayer Graphene Solutions. *Nat. Nanotechnol.* **2011**, *6*, 439–445.
- (28) Son, J. G.; Son, M.; Moon, K. J.; Lee, B. H.; Myoung, J. M.; Strano, M. S.; Ham, M. H.; Ross, C. A. Sub-10 nm Graphene Nanoribbon Array Field-Effect Transistors Fabricated by Block Copolymer Lithography. *Adv. Mater.* **2013**, *25*, 4723–4728.
- (29) Zhang, Y. B.; Tang, T. T.; Girit, C.; Hao, Z.; Martin, M. C.; Zettl, A.; Crommie, M. F.; Shen, Y. R.; Wang, F. Direct Observation of a Widely Tunable Bandgap in Bilayer Graphene. *Nature* **2009**, *459*, 820–823.
- (30) Park, J.; Jo, S. B.; Yu, Y. J.; Kim, Y.; Yang, W.; Lee, W. H.; Kim, H. H.; Hong, B. H.; Kim, P.; Cho, K.; et al. Single-Gate Bandgap Opening of Bilayer Graphene by Dual Molecular Doping. *Adv. Mater.* **2012**, *24*, 407–411.
- (31) Zhang, Y.; Small, J. P.; Pontius, W. V.; Kim, P. Fabrication and Electric-Field-Dependent Transport Measurements of Mesoscopic Graphite Devices. *Appl. Phys. Lett.* **2005**, *86*, 073104.
- (32) Kim, T.; Kim, H.; Kwon, S. W.; Kim, Y.; Park, W. K.; Yoon, D. H.; Jang, A. R.; Shin, H. S.; Suh, K. S.; Yang, W. S. Large-Scale Graphene Micropatterns Via Self-Assembly-Mediated Process for Flexible Device Application. *Nano Lett.* **2012**, *12*, 743–748.
- (33) Park, J. U.; Nam, S.; Lee, M. S.; Lieber, C. M. Synthesis of Monolithic Graphene-Graphite Integrated Electronics. *Nat. Mater.* **2012**, *11*, 120–125.
- (34) Han, J. T.; Jang, J. I.; Jeong, B. H.; Kim, B. J.; Jeong, S. Y.; Jeong, H. J.; Cho, J. H.; Lee, G.-W. Spontaneous Reduction and Dispersion of Graphene Nano-Platelets with in Situ Synthesized Hydrazine Assisted by Hexamethyldisilazane. *J. Mater. Chem.* **2012**, *22*, 20477–20481.
- (35) Lim, J. A.; Park, S. H.; Baek, J. H.; Ko, Y. D.; Lee, H. S.; Cho, K.; Lee, J. Y.; Lee, D. R.; Cho, J. H. Selectively Patterned Highly Conductive Poly(3,4-Ethylenedioxythiophene)-Tosylate Electrodes for High Performance Organic Field-Effect Transistors. *Appl. Phys. Lett.* **2009**, *95*, 233509.
- (36) Jeong, S. Y.; Kim, S. H.; Han, J. T.; Jeong, H. J.; Yang, S.; Lee, G. W. High-Performance Transparent Conductive Films Using Rheologically Derived Reduced Graphene Oxide. *ACS Nano* **2011**, *5*, 870–878.
- (37) Dreyer, D. R.; Park, S.; Bielawski, C. W.; Ruoff, R. S. The Chemistry of Graphene Oxide. *Chem. Soc. Rev.* **2010**, *39*, 228–240.
- (38) Chen, W. F.; Yan, L. F.; Bangal, P. R. Preparation of Graphene by the Rapid and Mild Thermal Reduction of Graphene Oxide Induced by Microwaves. *Carbon* **2010**, *48*, 1146–1152.
- (39) El-Kady, M. F.; Strong, V.; Dubin, S.; Kaner, R. B. Laser Scribing of High-Performance and Flexible Graphene-Based Electrochemical Capacitors. *Science* **2012**, *335*, 1326–1330.
- (40) Gilje, S.; Dubin, S.; Badakhshan, A.; Farrar, J.; Danczyk, S. A.; Kaner, R. B. Photothermal Deoxygenation of Graphene Oxide for Patterning and Distributed Ignition Applications. *Adv. Mater.* **2010**, *22*, 419–423.
- (41) Cote, L. J.; Cruz-Silva, R.; Huang, J. X. Flash Reduction and Patterning of Graphite Oxide and Its Polymer Composite. *J. Am. Chem. Soc.* **2009**, *131*, 11027–11032.
- (42) Han, W. S.; Hong, J. M.; Kim, H. S.; Song, Y. W. Multi-Pulsed White Light Sintering of Printed Cu Nanoinks. *Nanotechnology* **2011**, *22*, 395705.
- (43) Kang, H.; Sowade, E.; Baumann, R. R. Direct Intense Pulsed Light Sintering of Inkjet-Printed Copper Oxide Layers within Six Milliseconds. *ACS Appl. Mater. Interfaces* **2014**, *6*, 1682–1687.
- (44) Jin, H. Y.; Kim, J. Y.; Lee, J. A.; Lee, K.; Yoo, K.; Lee, D. K.; Kim, B.; Kim, J. Y.; Kim, H.; Son, H. J.; et al. Rapid Sintering of TiO<sub>2</sub> Photoelectrodes Using Intense Pulsed White Light for Flexible Dye-Sensitized Solar Cells. *Appl. Phys. Lett.* **2014**, *104*, 143902.
- (45) Yang, H. Y.; Hong, J. M.; Kim, T. W.; Song, Y. W.; Choi, W. K.; Lim, J. A. Split-Second Nanostructure Control of a Polymer:Fullerene Photoactive Layer Using Intensely Pulsed White Light for Highly Efficient Production of Polymer Solar Cells. *ACS Appl. Mater. Interfaces* **2014**, *6*, 1495–1501.
- (46) Ryu, S.; Liu, L.; Berciaud, S.; Yu, Y. J.; Liu, H. T.; Kim, P.; Flynn, G. W.; Brus, L. E. Atmospheric Oxygen Binding and Hole Doping in Deformed Graphene on a SiO<sub>2</sub> Substrate. *Nano Lett.* **2010**, *10*, 4944–4951.
- (47) Lee, W. H.; Park, J.; Kim, Y.; Kim, K. S.; Hong, B. H.; Cho, K. Control of Graphene Field-Effect Transistors by Interfacial Hydrophobic Self-Assembled Monolayers. *Adv. Mater.* **2011**, *23*, 3460–3464.
- (48) Wang, H.; Wu, Y.; Cong, C.; Shang, J.; Yu, T. Hysteresis of Electronic Transport in Graphene Transistors. *ACS Nano* **2010**, *4*, 7221–7228.
- (49) Latil, S.; Henrard, L. Charge Carriers in Few-Layer Graphene Films. *Phys. Rev. Lett.* **2006**, *97*, 036803.
- (50) McClure, J. W. Band Structure of Graphite and De Haas-Van Alphen Effect. *Phys. Rev.* **1957**, *108*, 612–618.
- (51) McAllister, M. J.; Li, J. L.; Adamson, D. H.; Schniepp, H. C.; Abdala, A. A.; Liu, J.; Herrera-Alonso, M.; Milius, D. L.; Car, R.; Prud'homme, R. K.; et al. Single Sheet Functionalized Graphene by Oxidation and Thermal Expansion of Graphite. *Chem. Mater.* **2007**, *19*, 4396–4404.
- (52) Ajayan, P. M.; Terrones, M.; de la Guardia, A.; Huc, V.; Grobert, N.; Wei, B. Q.; Lezec, H.; Ramanath, G.; Ebbesen, T. W. Nanotubes in a Flash - Ignition and Reconstruction. *Science* **2002**, *296*, 705–705.
- (53) Huang, J. X.; Kaner, R. B. Flash Welding of Conducting Polymer Nanofibres. *Nat. Mater.* **2004**, *3*, 783–786.
- (54) Lim, J. A.; Cho, J. H.; Park, Y. D.; Kim, D. H.; Hwang, M.; Cho, K. Solvent Effect of Inkjet Printed Source/Drain Electrodes on Electrical Properties of Polymer Thin-Film Transistors. *Appl. Phys. Lett.* **2006**, *88*, 082102.
- (55) Shen, X.; Ho, C.-M.; Wong, T.-S. Minimal Size of Coffee Ring Structure. *J. Phys. Chem. B* **2010**, *114*, 5269–5274.